Structure of nematic liquid crystalline elastomers under uniaxial deformation

Fan Zhang and Paul A. Heiney*
Department of Physics and Astronomy, University of Pennsylvania, Philadelphia, Pennsylvania 19104, USA

Amritha Srinivasan, Jawad Naciri, and Banahalli Ratna
Laboratory for Interfacial Interactions, Center for Bio/Molecular Science and Engineering, Code 6930, Naval Research Laboratory, Washington, DC 20375-5320, USA
(Received 19 May 2005; published 7 February 2006)

We have used *in situ* x-ray diffraction and calorimetry to study liquid crystalline elastomers prepared using a one-step photopolymerization method. We used suspended weights to stretch free-standing crystalline elastomer films. With the mechanical stress parallel to the initial director, we observed a gradual nematic to isotropic transition with increasing temperature. The thermal evolution of the nematic order parameter on cooling, together with the observation of isotropic-nematic coexistence over a broad temperature range, suggests that the heterogeneity in the samples introduces a distribution of transition temperatures. With the mechanical stress perpendicular to the initial director, we observed both uniform director rotation and stripe formation, depending on the details of sample preparation.

DOI: 10.1103/PhysRevE.73.021701 PACS number(s): 61.30.Gd, 61.41.+e, 64.70.Md, 61.10.Nz

INTRODUCTION

Liquid crystalline elastomers (LCE's) continue to attract attention due to their unusual physical properties [1–4] which have led to potential applications as actuators [5], artificial muscles [6,7], piezoelectrics [8], and optical-band materials [9]. Many of the structural properties of LCE's [10–16], such as high extensibility and spontaneous shape changes, arise from the coupling between mechanical deformation and director orientation [17,18].

To take full advantage of the optical, mechanical, and thermal properties of LCE's, highly oriented samples are required. Three approaches have been taken to the synthesis of monodomain or highly oriented LCE's: weak alignment followed by crosslinking [13], crosslinking prealigned polymers in a magnetic field [14], or one-step photopolymerization and crosslinking off of substrate-aligned monomers [6]. We have used x-ray diffraction (XRD) to study LCE's prepared according to the third method. Samples were stretched either parallel or perpendicular to the original direction orientation direction, and the structure was studied as a function of temperature.

EXPERIMENTAL SECTION

Materials

Mesogens MAOC4 (4″-Acryloyloxybutyl 2,5-Di (4′-butyloxybenzoyloxy)benzoate), MACC5 (4″-Acryloyloxybutyl 2,5-Di(4′-pentylcyclohexylcarboxyloxy) benzoate were synthesized as previously described [6] [Fig. 1(a)]. Crosslinker HDA (1,6-hexanedioldiacrylate) was obtained from Aldrich. Prior to polymerization, inhibitor hydroquinone was removed from HDA using an inhibitor removal column (Column DHR-4 from Scientific Polymer Products, Inc.).

To prepare free-standing films, 45 mole % each of MAOC4 and MACC5 mesogens were mixed with 10 mole % of HDA crosslinkers. The mixture was loaded into a glass alignment cell with a 50 μm gap at 25 mm Hg vacuum and $T=85$ °C. The cell walls were coated with poly(vinyl alcohol) (PVA) film, which was rubbed to introduce a preferred orientation for the mesogens. The cell was heated to 95 °C, then cooled at 1 °C/min to room temperature. Yellow light and nitrogen were applied during the cooling process to prevent photopolymerization. This process ensured the alignment of the mesogens. At 30 °C the photopolymerization process was carried out via a 5 minute light exposure of 0.97 mW using a 75 W Oriel xenon UV lamp equipped with a 365 nm cutoff filter. In this process, the mesogens were crosslinked and the elastomer network was formed. The schematic representation of the LCE is shown in scheme 1(b). The elastomer film was extracted from the glass cell by heating in distilled water at 80 °C–100 °C for 20 min. The obtained films were approximately 1 inch square, and were cut into smaller pieces for subsequent thermal, structural, and mechanical measurements.

Thermal analysis

Differential Scanning Calorimetry (DSC) measurements employed a TA Instruments 4100 Thermal Analyzer incorporating a 2920 Differential Scanning Calorimeter with modulated DSC module. The samples were cut into strips with approximate mass of 10 mg. Different films were subjected to 0, 10 kPa, 20 kPa, and 30 kPa external mechanical stresses for a period of 1 hour before the DSC measurements. Scans were performed at 3 °C/min between room temperature and 150 °C under a purified argon gas atmosphere with a flow rate of 80 mL/min.

*Corresponding author; Electronic address: heiney@sas.upenn.edu

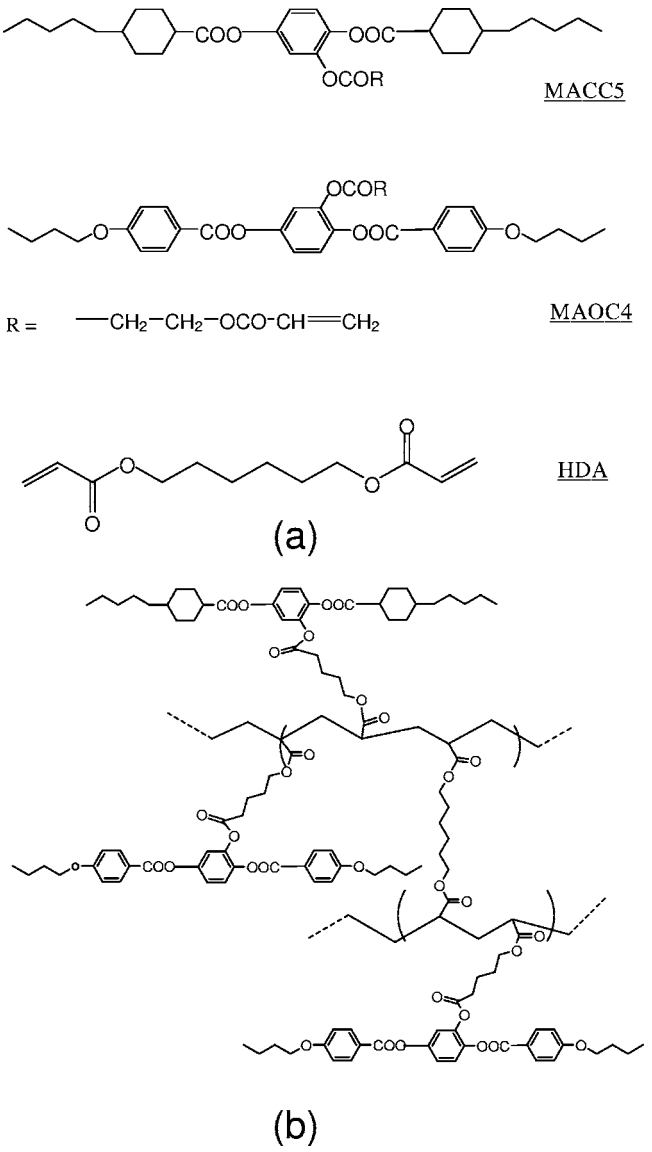

FIG. 1. (a) Chemical structures for the two monomers MACC5 and MAOC4, and the crosslinker HDA. (b) Schematic representation of the polymerized LCE.

X-ray scattering

X-ray diffraction (XRD) experiments utilized Cu$K_{\alpha 1}$ radiation from a rotating anode (Bruker AXS FR591) x-ray generator, focused and monochromatized via mirror-monochromator optics, and measured with a wire area detector (Bruker AXS Hi-Star), as previously described [19]. The size of the beam at the sample position was approximately 0.5×0.5 mm^2. The scattering geometry is shown in Fig. 2. To minimize attenuation and background scattering, an integral vacuum was maintained along the length of the flight tube and within the sample chamber. The sample temperature was controlled between room temperature and 150 °C to a precision of 0.25 °C.

For XRD measurements the films were cut into 3 mm $\times 10$ mm strips with a thickness of 50 μm. The sample width and length were accurate to 0.1 mm. For *in situ* strain measurements, each sample was clamped at its upper end to an aluminum block, and at the bottom end calibrated weights were clamped to the sample. Measurements were made with the gravitationally induced stress either parallel or perpendicular to the original director orientation, as shown schematically in Figs. 2 and 3. To prevent sample breakage it was important to distribute the load as uniformly as possible by padding the clamps with kapton tape and aluminum foil. The sample length was monitored *in situ* to an accuracy of 1% by measuring the attenuation of the primary x-ray beam through the sample as a function of vertical translation. We also made measurements on a 1:1 monomer mixture of MAOC4 to MACC5 (no crosslinker). The mixture was loaded in a glass capillary with a diameter of 1 mm. It was subsequently heated to 120 °C, which is above the nematic-isotropic (NI) transition temperature for the liquid crystal mesogens. We cooled the monomer mixture sample in a 0.5 T magnetic field at the rate of 1 °C/min and made the measurements at room temperature.

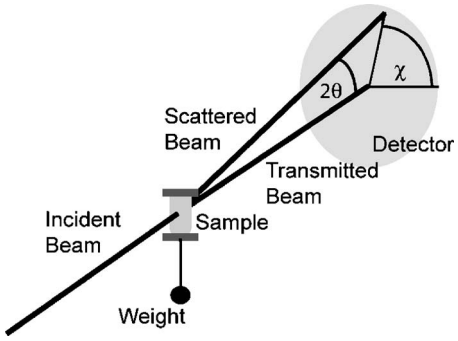

FIG. 2. Schematic illustration of the x-ray diffraction geometry. χ is the azimuthal angle and 2θ is the scattering (Bragg) angle.

Analysis

The primary goal of the structural measurements was to obtain the orientational distribution of molecular long axis orientations (which are closely related to the optical directors) from the XRD patterns. For each diffraction pattern, the azimuthal (polar) distribution of the diffracted intensity, $I(\chi)$, at a selected momentum transfer (corresponding to either the small-angle or the wide-angle nematic peak) was extracted using Datasqueeze [20]. At each value of χ, we integrated over q such that 95% of the scattered intensity was included.

Extraction of the molecular axis distribution from the x-ray intensity distribution is complicated by several factors: (a) The molecules have an orientational distribution within each domain, and there is also a separate distribution of domain orientations. The measured orientation distribution depends on the convolution of these two effects. (b) Even for absolutely uniform molecular orientations (order parameter of unity) there will be a finite angular width to the x-ray diffraction feature due to the size and shape of the molecules. We will discuss first our approach to the second problem.

Although, in principle, once the single molecular form factor is known, the orientational distribution function can be obtained by expanding the azimuthal intensity distribution

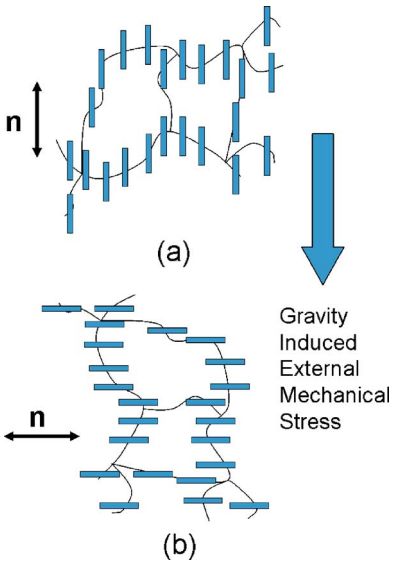

FIG. 3. (Color online) Schematic illustration of parallel and perpendicular configurations. In the parallel configuration (a) the sample is stretched parallel to the direction of the mean starting director orientation, while in the perpendicular orientation (b) the two directions are orthogonal.

into Legendre polynomials [21], this method requires a high-order expansion of the Legendre polynomials. In our analysis, we instead followed the procedure of Leadbetter and Norris [22], who assumed that the molecules are rotationally symmetric rods of infinite length and that the molecular long axes are uniformly oriented within each domain. If α is the angle of a particular molecular axis with respect to the z axis, and $D(\alpha)$ is the distribution function describing the axis orientations, then the azimuthal distribution of XRD intensity is given [22] by

$$I(\chi) = I_0 \int_{\chi}^{\pi/2} \frac{D(\alpha)\sin\alpha}{\cos^2\chi\sqrt{\tan^2\alpha - \tan^2\chi}} d\alpha. \tag{1}$$

Here the orientational distribution functions are properly normalized to unity and I_0 is a prefactor relating the absolute XRD intensity to the relative intensity.

Accounting for the distinction between the domain distribution function $D^d(\alpha)$ and the single molecule distribution function, $D(\alpha)$ is more complicated. However, for relatively low order parameters less than 0.8, previous experiments [23–26] have indicated that the difference between these two functions is small, in part because the long axis fluctuations are dominated by collective fluctuations of many molecules. We note that the surfacing anchoring we employed to align the liquid crystal mesogen before crosslinking does not remove the director fluctuations completely. This approach is different from the most widely applied two-step synthesis of Finkelmann [13], which is expected to yield better aligned samples.

We used the common approach [27] of least-squares fitting our measured $I(\chi)$ to an empirical distribution function $D(\alpha)$. Conventional theory assumes that, away from the transition region, the entire sample is nematic. However, we observed an isotropic component to the orientational distribution even at the lowest temperatures measured, which could not be described by conventional distribution functions. We therefore tested several empirical distribution functions, consisting of Gaussian [28], modified Onsager [29], or Maier-Saupe [31], trial distribution functions with an additional constant term, as shown below. (The Oldenbourg function [30] can also be expressed using the Maier-Saupe function with modified parameters).

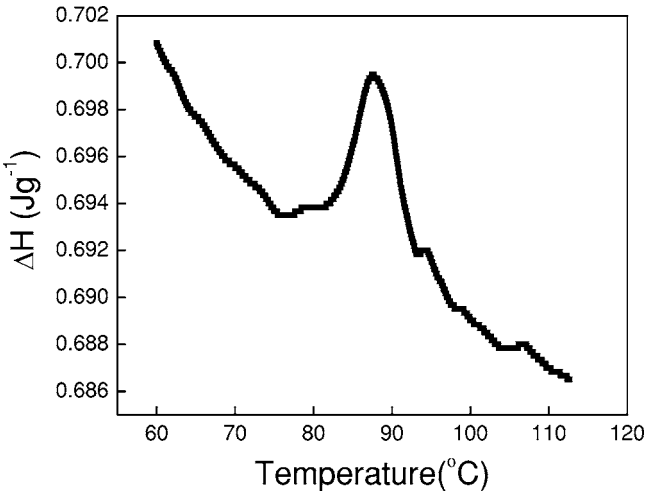

FIG. 4. DSC scan performed at heating rate of 3 °C/min. The peak shown in the figure can be fit to a Gaussian curve with center at 87.5 °C and Gaussian width of 4.67 °C.

$$D(\alpha) = C + A \times \begin{cases} \exp(-\alpha^2/2m^2) & \text{(Gaussian)}, \\ \exp(m\cos\alpha^2) & \text{(Maier-Saupe)}, \\ \dfrac{m\cosh(m\cos\alpha)}{4\pi m\sinh m} & \text{(Onsager)}. \end{cases} \tag{2}$$

Here A is proportional to the total fraction of mesogens in the nematic phase, C is proportional to the fraction of mesogens in the isotropic phase, and m is a measure of the width of the distribution. After the normalized orientational distribution function has been obtained, it is Legendre averaged to obtain the nematic order parameter of order $2n$,

$$S_{2n} = \int D(\alpha)P_{2n}(\cos\alpha)d\cos\alpha. \tag{3}$$

EXPERIMENTAL RESULTS AND DISCUSSION

DSC results

Figure 4 shows a typical DSC scan. We observe only one peak in the measured temperature range, corresponding to the nematic-to-isotropic phase transition. The peak can be fitted to a smooth background plus Gaussian curve,

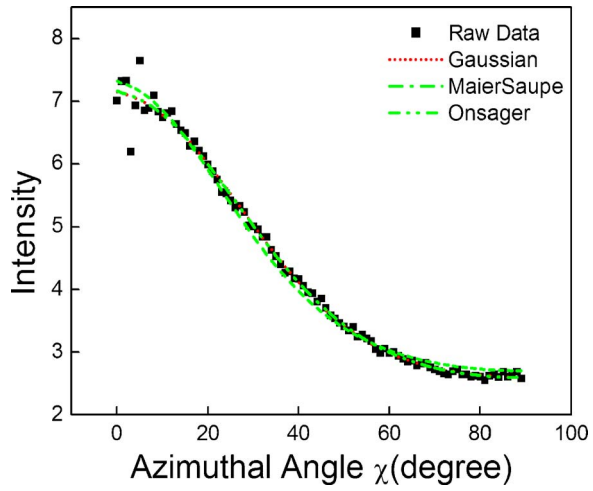

FIG. 5. (Color online) $I(\chi)$ profile for MAOC4-MACC5 sample in the parallel configuration with a 30 kPa external stress at 80 °C. The raw data are shown by solid squares, curves show best-fit results to trial orientational functions (incorporating an adjustable constant term) as discussed in the text [Eq. (2)].

$$I = I_0 + \frac{I_1}{T} + \frac{I_2}{T^2} + \frac{C}{\sigma\sqrt{2\pi}} \exp\left[-\frac{1}{2}\left(\frac{T - T_c}{\sigma}\right)^2\right] \qquad (4)$$

with center at T_c=87.5 °C and Gaussian width σ=4.67 °C. The thermal stability of our samples was manifested by the reproducibility of thermal behavior on successive heat-cool cycles. Thermal measurements made at zero stress both before and after stretching showed little evidence of history-dependent behavior, with no dependence on mechanical history of either T_c or σ. This indicates that the relaxation processes in our samples were relatively fast and/or that the transition temperature distribution was not highly sensitive to applied stress.

XRD measurements in the parallel configuration

XRD measurements were made at a variety of applied stresses and temperatures, and the orientational distribution functions obtained as discussed above. As shown in Fig. 5, all three trial distribution functions fit the measured intensity distribution well, with temperature-dependent normalization factors $A(T)$ and $C(T)$ and temperature-dependent distribution widths $m(T)$. This agreement is consistent with Hamley's prediction that x-ray patterns should be insensitive to higher-order terms in the spherical harmonic expansion of the orientational distribution functions [32]. By contrast, a recent Monte Carlo simulation of hard spherocylinders [33] found that the best fit to the orientational distribution function was given by the Maier-Saupe form when nematic director fluctuations were not considered and by the Gaussian form when the fluctuations were taken into account. In our system, it is likely the thermal fluctuations are suppressed by crosslinking and should have a relatively small effect on the orientational distribution function.

We used the normalization factors from fitted orientational distribution function to calculate the percentage of mesogens in the nematic and isotropic phases. Ideally, all molecules should be in the nematic phase below the transition temperature, and in the isotropic phase above T_c. In fact, as shown in Fig. 6, almost 55% of the mesogens are randomly oriented even at the lowest temperatures studied. A similar analysis of the magnetic field aligned monomer sample shows that at room temperature only 16% of the mesogens are randomly oriented. Thus, the high degree of orientational disorder in the elastomer sample is a direct result of the crosslinking process. A typical azimuthal intensity distribution profile is shown in Fig. 7. The isotropic fraction increases slowly with increasing temperature, with a rapid jump near the nominal transition temperature. Even well

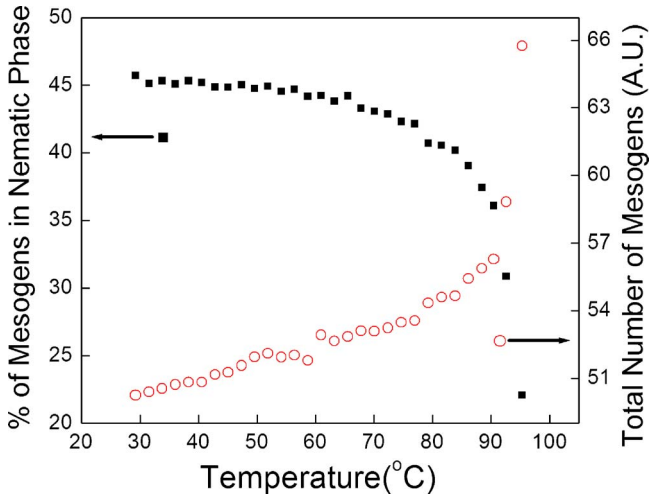

FIG. 6. (Color online) Calculated percentage of mesogens in nematic phase as a function of temperature, and sum of normalized integrated intensities of nematic and isotropic components of XRD intensity measured in the parallel configuration with 30 kPa external stress. This sum should be proportional to the total number of scatterers; its increase with temperature is believed to arise from sample thickening upon contraction.

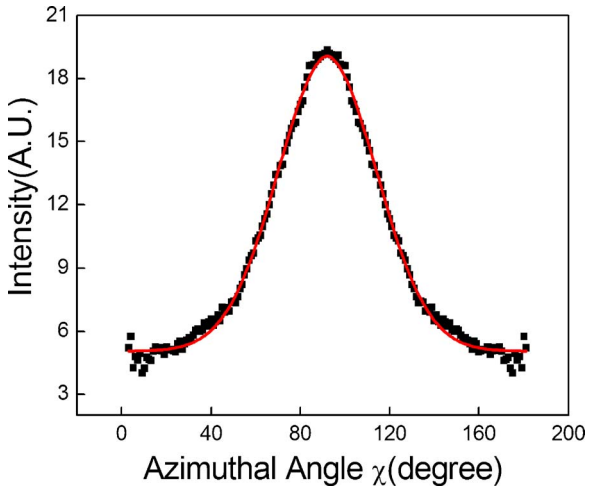

FIG. 7. (Color online) $I(\chi)$ profile for magnetically aligned MAOC4-MACC5 monomer sample, measured at room temperature. The XRD pattern was collected at room temperature. The solid curve shows the best fit from the orientational distribution analysis.

above the nominal transition temperature, however, the diffraction pattern shows some anisotropy, with approximately 20% of the molecules displaying nematic order. These observations indicate that our materials are quite heterogeneous. (Again, as discussed above, our data analysis does not unambiguously distinguish between the distribution of molecular directors within each domain and the distribution of domain orientations).

By carefully comparing the measured XRD intensities with properly normalized distribution functions, we can also extract a renormalized integrated intensity that should be proportional to the total number of mesogens in the x-ray beam, independent of the thermodynamic phase. As shown in Fig. 6, this intensity increases slowly with increasing temperature through the nematic phase, and then jumps dramatically at the phase transition. This intensity increase is consistent with our measurements of sample length versus temperature at fixed stress [Fig. 8(a)]. The samples shorten with increasing temperature along the direction of the uniaxial stress. (Regrettably, because of necking effects the sample length cannot be simply equated to the microscopic strain, but the strain should increase monotonically with increasing sample length.) Under the assumption of constant volume per mesogen, the samples should therefore thicken with increasing temperature, resulting in a larger total scattering cross section because there are more mesogens in the beam. The exact length dependence of scattered intensity is complicated: near the clamps at the ends of the sample the transverse width is fixed and the intensity should be inversely proportional to the length, but in the center of the sample the transverse sample dimension should also increase.

The $n=2$ order parameter obtained from Eq. (3) is commonly referred to as the "nematic order parameter" S_2, although in the present case it may more accurately represent the mosaic distribution of ordered domain orientations. Figure 8(b) shows a typical plot of S_2 versus temperature. S_2 decreases rapidly close to the transition temperature of 87.5 °C obtained by DSC. In a conventional thermotropic nematic, we expect a first-order NI transition, with a discontinuity in the order parameter at the transition temperature [34]. We observe instead a rapid but continuous evolution across the NI transition temperature. The most likely explanation is that the heterogeneity induced by the crosslinkers results in an effective distribution of transition temperatures, as proposed by Selinger *et al.* [4]. Quenched heterogeneity can result both from nonuniformities in the rubbing process and from variations in the crosslinker density. These effects, especially the chemical heterogeneity, result in quenched disorder in the LCE sample, which in turn gives rise to a statistical distribution of transition temperatures, with different domains undergoing the NI transition at different temperatures. This explanation is supported by a recent theoretical work [35] based on Monte Carlo simulations of a lattice model, which confirmed the heterogeneity determines the width of the NI transition in LCE's.

In order to quantitatively analyze the temperature dependence of the order parameter, we assume a Gaussian distribution of transition temperatures:

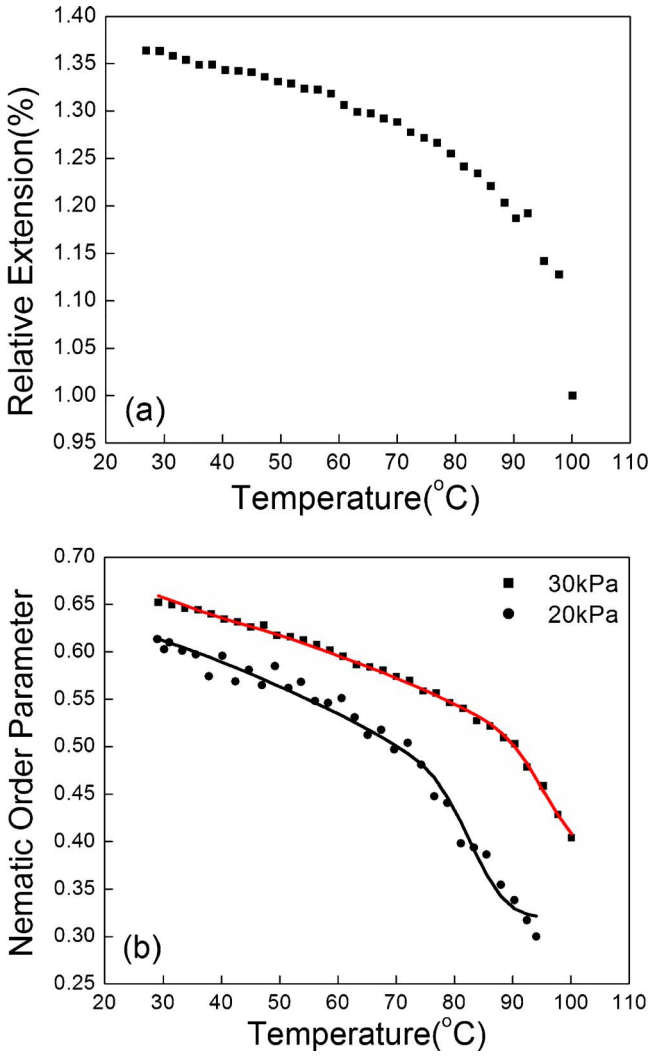

FIG. 8. (Color online) Temperature dependence of (a) fractional extension of MAOC4-MACC5 film under uniaxial mechanical stress of 30 kPa in the parallel configuration and (b) nematic order parameter on cooling with 30 kPa and 20 kPa external mechanical stresses. In (b), the solid curve shows the best fit to Eq. (7). Best fit parameters are $a=0.0306\pm0.0006$, $\delta=10.9\pm1.0$, $T_0=96.1\pm0.5$, and $S_0=0.384\pm0.006$ for 30 kPa and $a=0.0363\pm0.0014$, $\delta=11.7\pm3.1$, $T_0=83.5\pm1.0$, and $S_0=0.319\pm0.008$ for 20 kPa.

$$P(T_c)=\frac{1}{\sigma\sqrt{2\pi}}\exp[-(T_c-T_0)^2/2\sigma^2], \tag{5}$$

where T_c is the NI transition temperature of a given domain, σ is the distribution width, and T_0 is the mean transition temperature. We further assume that, within each domain, the NI transition is first-order but with a power law precursor, so that the nematic order parameter within the domain, S_{2d}, varies as

$$S_{2d}(T,T_c,\delta)=\begin{cases} a\left(\dfrac{T_c+\delta-T}{T_c}\right)^{\beta}, & T\leqslant T_c, \\ 0, & T>T_c, \end{cases} \tag{6}$$

where a is the saturation order parameter and δ is a temperature-independent offset. Finally, we must incorporate

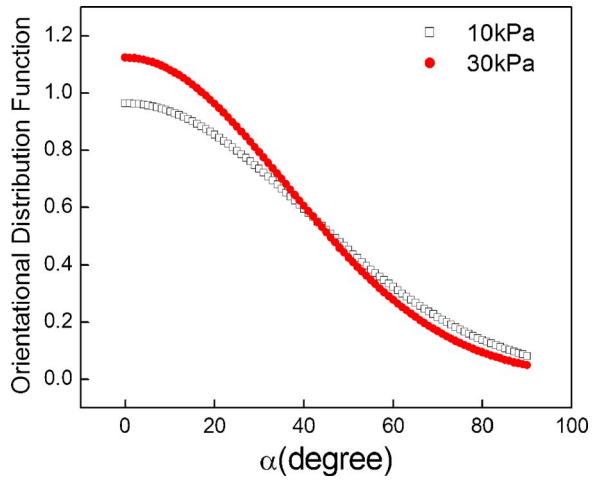

FIG. 9. (Color online) Orientational distribution functions measured at room temperature in the perpendicular orientation with 10 kPa and 30 kPa external stress.

the observation of nonzero order parameter above the nominal transition temperature, which must arise from the orienting effect of the mechanical field on the isotropic phase. Therefore, our final empirical expression for the measured order parameter S_2 is then given by a numerical convolution of Eqs. (5) and (6),

$$S_2(T) = S_0 + \frac{1}{\sigma\sqrt{2\pi}} \int dT_c S_{2d}(T, T_c, \delta) \exp\left(-\frac{(T_c - T_0)^2}{2\sigma^2}\right), \tag{7}$$

where S_0 represents a constant contribution to the order parameter.

We refined the model parameters via least-squares fits to the data. To reduce the number of fitting parameters, we fixed the width of the transition temperature distribution to be $\sigma = 4.67\ ^\circ\mathrm{C}$, as determined from DSC measurements, and fixed the critical exponent β at the theoretical value of 0.5 as predicted by the Landau-de Gennes mean field theory [36]. This left adjustable parameters of a, δ, T_0, and S_0. As shown in Fig. 8(b), the agreement between model and data is quite good. We were able to use the same value of σ for all applied stresses, consistent with our hypothesis that the apparently smooth NI transition results from microscopic heterogeneity quenched in during the fabrication process.

The model described in Eq. (7) incorporates a nonzero "residual order parameter" S_0 to account for the finite alignment observed even at the highest temperatures. This residual alignment is both from the applied stress and from the "mechanical field" induced by the original alignment. The stress dependence of S_0 is manifested by the observation [Fig. 8(b)] that, at any given temperature S_0 is larger for samples subjected to higher stress.

The fitted value of T_0 increases monotonically from 83.5 °C at 20 kPa external stress to 96.1 °C at 30 kPa external stress. This is as expected, since a higher degree of low-temperature director alignment implies more enthalpy from the transition to the isotropic phase and hence a higher transition temperature.

XRD measurements in the perpendicular configuration

Many of the unique properties of LCE's are believed to arise from coupling between macroscopic deformations of the sample and microscopic director reorientations [37]. Liquid crystalline elastomers can extend along the stretching direction with little or no elastic energy cost (an effect known as "soft elasticity") when the applied stress is not parallel to the quenched-in direction orientation [37,44]. Accompanying the extension is a characteristic director reorientation. In this section we discuss measurements in which the applied stress was approximately perpendicular to the original rubbing direction.

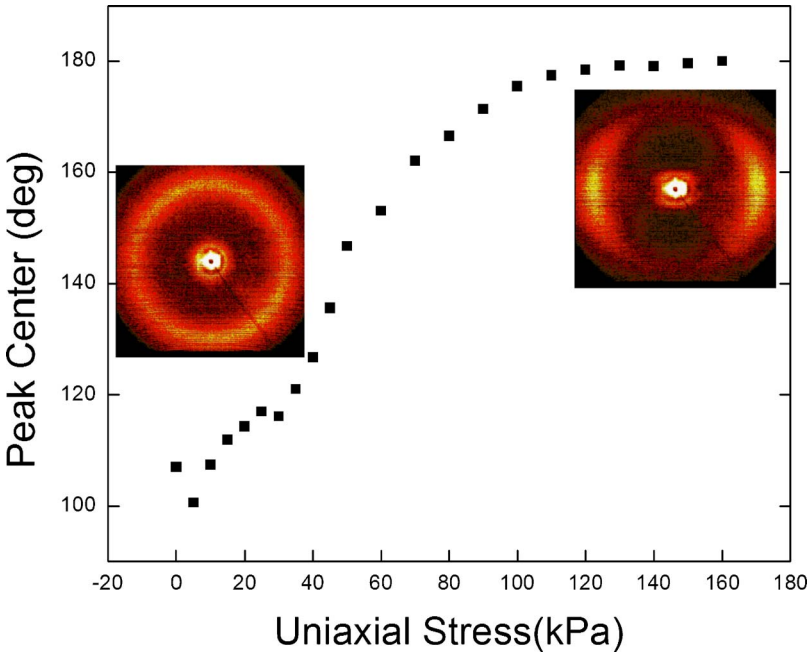

FIG. 10. (Color online) Fitted center of the wide-angle diffraction peak versus external weight at room temperature, measured in the perpendicular configuration. Insets show XRD patterns collected with stresses of 0 and 160 kPa.

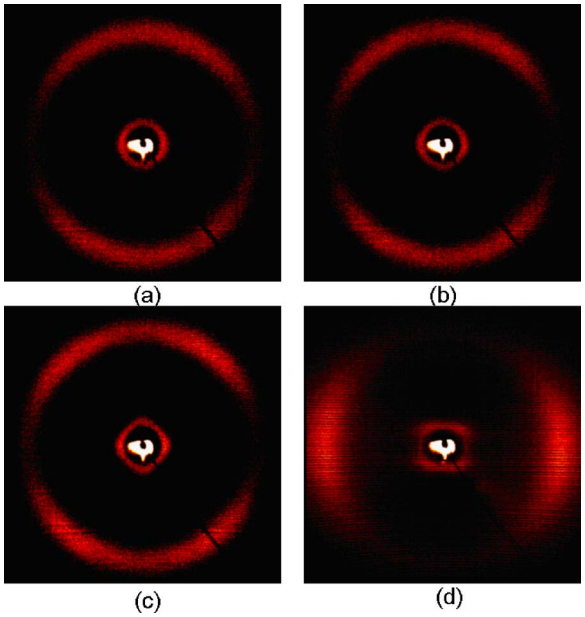

FIG. 11. (Color online) Room temperature XRD patterns collected at different external stresses in the perpendicular configuration. External stress is (a) 0, (b) 20 kPa, (c) 40 kPa, (d) 100 kPa.

As seen in previous experimental [10–12,14,38,39] and theoretical [16,18,40–42] studies, when a monodomain sample experiences a stress that is not coincident with the original direction orientation, the system can evolve to a final aligned state *via* two distinctive processes. The director can rotate uniformly and continuously, or a spontaneous distortion can arise in which periodic stripes with alternating orientations are arranged perpendicular to the uniform director axis. The characteristic length scale of the stripes is on the order of microns. Both behaviors can be observed either via optical microscopy (with crossed polarizers) or via XRD. In an XRD measurement, continuous director rotation is manifested as a continuous azimuthal rotation of the wide-angle diffuse maxima, while stripe formation is manifested as a splitting of the wide-angle feature into four distinct peaks. The different reorientation phenomena have been explained in terms of differences in chemical structure [10,14] and geometrical shape [43].

For XRD measurements in the perpendicular configuration, 4×10 mm^2 samples were cut out of larger films, with the long axis approximately perpendicular to the original rubbing direction. A weight was hung along the long axis of the film to provide the external stress. Transmission XRD measurements were then made at room temperature as a function of applied weight. The calibrated external stress was increased gradually from 0 kPa to 160 kPa, beyond which the sample broke. We then extracted the azimuthal (χ) dependence of the x-ray intensity in the vicinity of the wide-angle diffraction peak ($q=1.36$ Å^{-1}), and from that obtained the orientational distribution function (assuming a sum of Gaussian distributions) and the nematic order parameter as described in the preceding section.

In the unextended sample, we observed diffraction maximum at $\chi=90°$ and 270°, as expected. For a highly extended sample, we would expect diffraction maximum near at $\chi=0°$ and 180°.

In many samples, we observed uniform rotation of the molecular long axis orientation with increasing weight. Figure 9 shows the orientational distribution functions $D(\alpha)$ from such a sample, with 10 kPa and 30 kPa external stress, and Fig. 10 shows the reorientation of the molecular long axis. We observe that with increasing stress the distribution function becomes narrower, indicating a substantially higher degree of alignment, and also that the average orientation direction changes, indicating a rotation of the molecular long axes. To quantify the evolution of peak position with external weights, we performed least-squares fits of the wide-angle peak $I(\chi)$ to a Gaussian line shape. The fitted peak positions, together with representative false-color images, are shown in Fig. 10. With increasing weight, the peak sharpens and rotates from $\chi=100°$ to $\chi=180°$. The curve is sigmoidal, with saturation of the rotation starting at a stress at around 100 kPa, but peak sharpening continuing beyond that.

In some samples that had the same dimension and were cut from the same LCE film, instead of uniform orientation, we observed a stripe domain structure. Figure 11 shows typical false-color images from such a sample. At zero stress, the molecular long axis is oriented along the horizontal direction, resulting in diffraction maxima along the vertical axis. With increasing stress, the reflection splits in two, and the split reflections rotate towards the horizontal axis. The split reflections start to merge at a stress at around 60 kPa. When the stress is greater than 100 kPa, the four reflections merge into two new distinctive reflections along the horizontal axis.

We observed both director rotation and stripe domains in our measurements, but only one or the other in any given sample. Our samples all had the same dimensions and were cut from the same batch of free-standing elastomer film, so it is unlikely that crosslinker geometry or density were important determining factors. We believe instead that the sample morphology is primarily determined by the precise orientation of the external stress relative to the rubbing. When the two directions are close to perpendicular, different domains in the sample will spontaneously break the symmetry with different signs, resulting in a stripe domain structure. When the angle between the two directions deviates more substantially from 90°, the symmetry is already broken, and only one of the two rotation directions is selected. Future experiments to test this hypothesis will require more precise control of the exact direction of external stress relative to the director.

CONCLUSIONS

We have used XRD to probe director orientations in MAOC4-MACC5 as a function of temperature and uniaxial stress. The XRD patterns have isotropic- and nematic-like contributions that all temperatures, with a rapid evolution from nematic to an isotropic phase which can be described by a smeared first-order transition with a power-law precursor. The width of the transition measured by calorimetry is consistent with the smearing of the order parameter curve obtained by XRD.

In the perpendicular configuration, we observed both uniform rotations and stripe domains in different samples under nominally identical preparation conditions. In samples displaying uniform rotation, we observed a slow rotation of the direction as a function of external stress, rather than a sharp transition as shown in Ref. [14]. We also found that the degree of alignment increases with increasing stress, as expected. We suggest that the tendency towards stripe domain or director rotation are determined more by the relative orientations of the starting director orientation and the external stress than by microscopic effects such as crosslinker density.

ACKNOWLEDGMENTS

The authors acknowledge the Office of Naval Research for financial support. The authors thank T. C. Lubensky for useful discussions, and J. M. Kikkawa and Roger I. Miller for assistance with magnetic alignment.

[1] P. G. de Gennes, Comptes Rendus Hebdomadaires des Seances de L academie des Sciences Serie B **281**, 101 (1975).
[2] A. R. Tajbakhsh and E. M. EM, Eur. Phys. J. E **6**, 181 (2001).
[3] H. Finkelmann, A. Greve, and M. Warner, Eur. Phys. J. E **5**, 281 (2001).
[4] J. V. Selinger, H. G. Jeon, and B. R. Ratna, Phys. Rev. Lett. **89**, 225701 (2002).
[5] J. Naciri, A. Srinivasan, H. G. Jeon, N. Nikolov, P. Keller, and B. R. Ratna, Macromolecules **36**, 8499 (2003).
[6] D. L. Thomsen, P. Keller, J. Naciri, P. Pink, H. G. Jeon, D. K. Shenoy, and B. R. Ratna, Macromolecules **34**, 5868 (2001).
[7] D. K. Shenoy, D. L. Thomsen, A. Srinivasan, P. Keller, and B. R. Ratna, Sens. Actuators, A **96**, 184 (2002).
[8] W. Meier and H. Finkelmann, Makromolekulare Chemie-Rapid Communications **11**, 599 (1990).
[9] P. A. Bermel and M. Warner, Phys. Rev. E **65**, 056614 (2002).
[10] I. Kundler and H. Finkelmann, Makromolekulare Chemie-Rapid Communications **16**, 679 (1995).
[11] I. Kundler, E. Nishikawa, and H. Finkelmann, Macromol. Symp. **117**, 11 (1997).
[12] I. Kundler and H. Finkelmann, Macromol. Chem. Phys. **199**, 677 (1998).
[13] J. Kupfer and H. Finkelmann, Makromolekulare Chemie-Rapid Communications **12**, 717 (1991).
[14] G. R. Mitchell, F. J. Davis, and W. Guo, Phys. Rev. Lett. **71**, 2947 (1993).
[15] H. M. Brodowsky, E. M. Terentjev, F. Kremer, and R. Zentel, Europhys. Lett. **57**, 53 (2002).
[16] P. Bladon, E. M. Terentjev, and M. Warner, Phys. Rev. E **47**, R3838 (1993).
[17] T. C. Lubensky, R. Mukhopadhyay, L. Radzihovsky, and X. J. Xing, Phys. Rev. E **66**, 011702 (2002).
[18] M. Warner and E. M. Terentjev, Prog. Polym. Sci. **21**, 853 (1996).
[19] V. Percec, T. K. Bera, M. Glodde, Q. Fu, V. S. K. Balagurusamy, and P. A. Heiney, Chem.-Eur. J. **2003**, 921 (2003).
[20] The *Datasqueeze* data analysis software is available at http://www.datasqueezesoftware.com
[21] H. D. Deas, Acta Crystallogr. **5**, 542 (1952).
[22] A. J. Leadbetter and E. K. Norris, Mol. Phys. **38**, 669 (1979).
[23] R. M. Richardson, J. M. Allman, and G. R. McIntyre, Liq. Cryst. **7**, 701 (1990).
[24] Z. X. Fan, S. Buchner, W. Haase, and H. G. Zachmann, J. Chem. Phys. **92**, 5099 (1990).
[25] W. Haase, Z. X. Fan, and H. J. Muller, J. Chem. Phys. **89**, 3317 (1988).
[26] D. Bauman, Z. X. Fan, and W. Haase, Liq. Cryst. **6**, 239 (1989).
[27] K. R. Purdy, Z. Dogic, S. Fraden, A. Ruhm, L. Lurio, and S. G. J. Mochrie, Phys. Rev. E **67**, 031708 (2003).
[28] T. Odijk, Macromolecules **19**, 2314 (1986).
[29] L. Onsager, Ann. N.Y. Acad. Sci. **51**, 627 (1949).
[30] R. Oldenbourg, X. Wen, R. B. Meyer, and D. L. D. Caspar, Phys. Rev. Lett. **61**, 1851 (1988).
[31] W. Maier and A. Saupe, Z. Naturforsch. A **13A**, 564 (1958).
[32] I. W. Hamley, J. Chem. Phys. **95**, 9376 (1991).
[33] S. V. Savenko and M. Dijkstra, Phys. Rev. E **70**, 011705 (2004).
[34] P. G. de Gennes, *The Physics of Liquid Crystals* (Oxford University Press, Oxford, 1993).
[35] J. V. Selinger and B. R. Ratna, Phys. Rev. E **70**, 041707 (2004).
[36] P. M. Chaikin and T. C. Lubensky, *Principles of Condensed Matter Physics* (Cambridge University Press, Cambridge, 1995).
[37] M. Warner and E. M. Terentjev, *Liquid Crystalline Elastomers* (Oxford University Press, Oxford, 2003).
[38] J. Kupfer and H. Finkelmann, Macromol. Chem. Phys. **195**, 1353 (1994).
[39] H. Finkelmann, I. Kundler, E. M. Terentjev, and M. Warner, J. Phys. II **7**, 1059 (1997).
[40] G. C. Verwey, M. Warner, and E. M. Terentjev, J. Phys. II **6**, 1273 (1996).
[41] P. Bladon, M. Warner, and E. M. Terentjev, Macromolecules **27**, 7067 (1994).
[42] J. Weilepp and H. R. Brand, Europhys. Lett. **34**, 495 (1996).
[43] R. V. Talroze, E. R. Zubarev, S. A. Kuptsov, A. S. Merekalov, T. I. Yuranova, N. A. Plate, and H. Finkelmann, React. Funct. Polym. **41**, 1 (1999).
[44] M. Warner, P. Bladon, and E. M. Terentjev, J. Phys. II **4**, 93 (1994).